GSA Data Repository 2020123

Doran, A.K., and Crawford, W.C., 2020, Continuous evolution of oceanic crustal structure following an eruption at Axial Seamount, Juan de Fuca Ridge: Geology, v. 48, https://doi.org/10.1130/G46831.1

Supplemental figures for:

Continuous evolution of oceanic crustal structure following an eruption at Axial Seamount, Juan de Fuca Ridge

Adrian K. Doran[1] and Wayne C. Crawford[2]

[1]*Institution of Geophysics and Planetary Physics, Scripps Institution of Oceanography, University of California San Diego, 9500 Gilman Drive, La Jolla, CA 92093, USA*

[2]*Laboratorie de Géosciences Marines, Institut de Physique du Globe de Paris, 4 Place Jussieu, 75252 Paris, France*

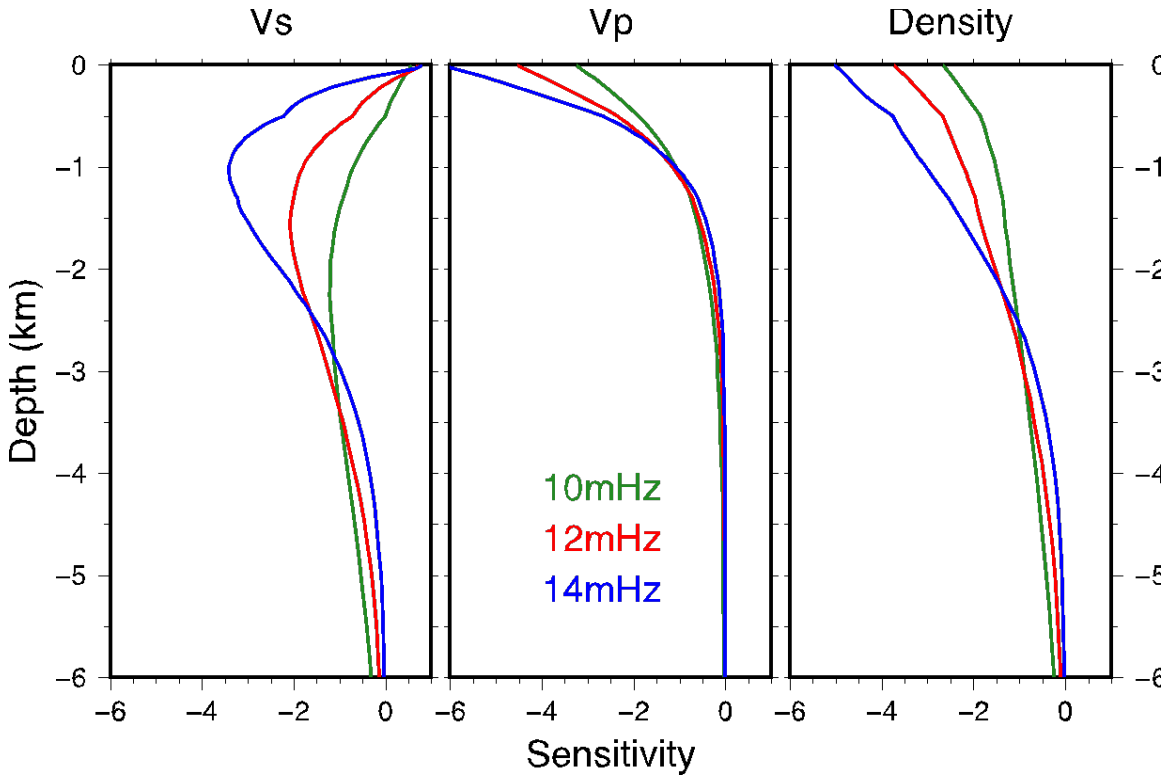

Supplemental Figure S1. Sensitivity of seafloor compliance data to a fractional change in crustal properties as a function of depth. Sensitivity functions are computed for individual frequencies (shown in different colors) from a starting model of typical oceanic crust. In this study we solve for shear velocity (Vs) and assume models of compressional velocity (Vp) and density from the results of Arnulf et al (2018).

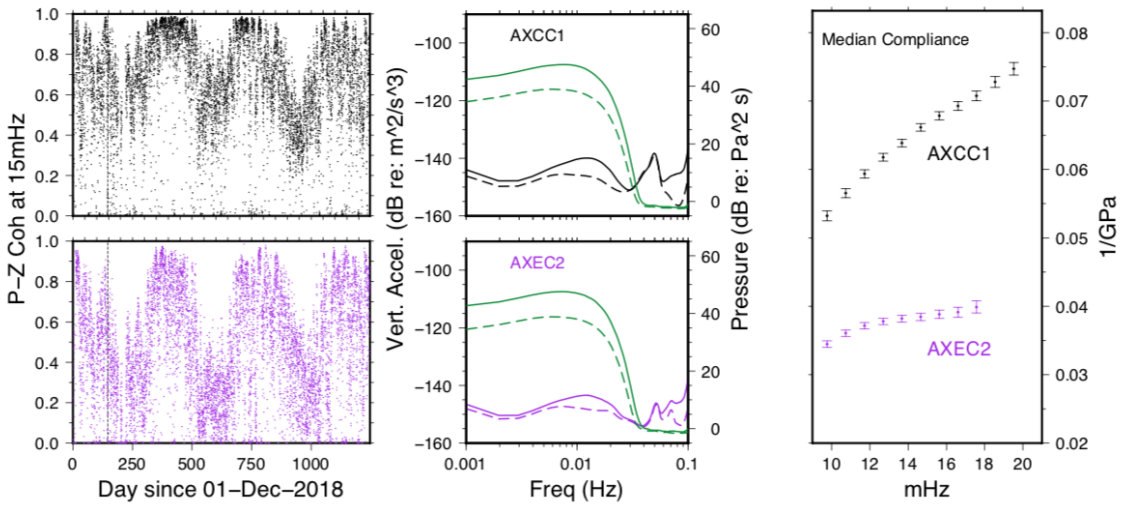

Supplemental Figure S2. Left panels: Magnitude-squared coherence between vertical acceleration and pressure at 15 mHz as a function of time at AXCC1 (black) and AXEC2 (purple). The coherence peaks in the winters, when the infragravity signal is stronger, and decreases in the summers. The lower overall coherence observed at AXEC2 is indicative of lower signal-to-noise ratio at this site. Middle panels: Median vertical acceleration (purple and black lines) and pressure (green lines) spectra recorded during Summer 2016 (dashed lines) and Winter 2017 (solid lines) at both stations. Right panel: median seafloor compliance values calculated at AXCC1 and AXEC2 for the entire 3.5 year time period considered.

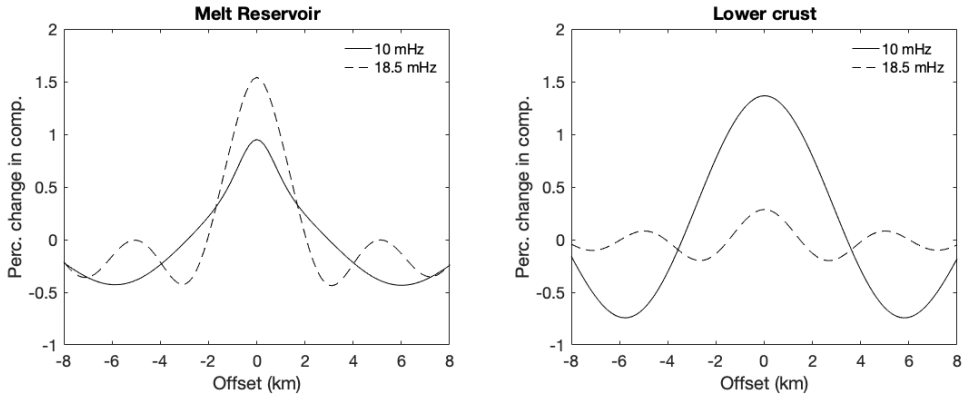

Supplemental Figure S3. Effects on compliance data as a function of frequency and geographic offset due to changes in subsurface structure. Modeling was performed using the semi-analytic solution of Hulme et al (2005), which considers the effect of a buried sphere in a homogenous half-space. We assumed basalt properties described in Figure S4. The left panel shows the effect of a change in the properties of the melt reservoir, simulated by a sphere of radius 500 meters buried at a depth of 2000 meters below the seafloor. The right panel shows the effect of a change in the properties of the lower crust, simulated by a sphere of radius 500 meters buried at a depth of 3500 meters below the seafloor. The vertical axis in both panels shows the percent change in compliance. The amplitude variations with offset demonstrate the increasing sampling radius of compliance data with decreasing frequency. If the inverted variations in lower crustal Vs were widespread, the effects would be visible at both AXCC1 and AXEC2, which was not observed.

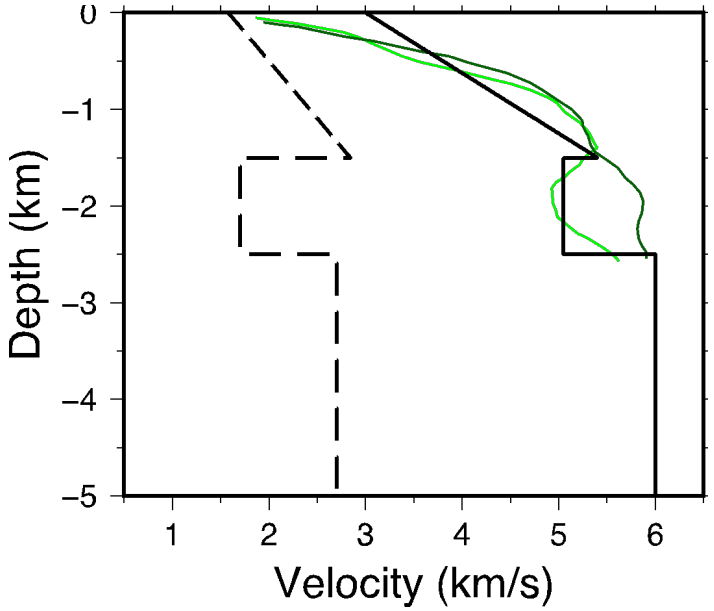

Supplemental Figure S4. Starting model for the Bayesian inversion of compliance data at AXCC1 and AXEC2. Vp is shown in the solid black line, Vs is shown in the dashed black line. The green lines show Vp profiles of Arnulf et al (2018) within the caldera (light green) and outside the caldera (dark green). Vs was initially set assuming a Poisson's ratio of 0.3. Density was scaled to Vp. Although not shown, the crust in our model extends to 11 km depth.

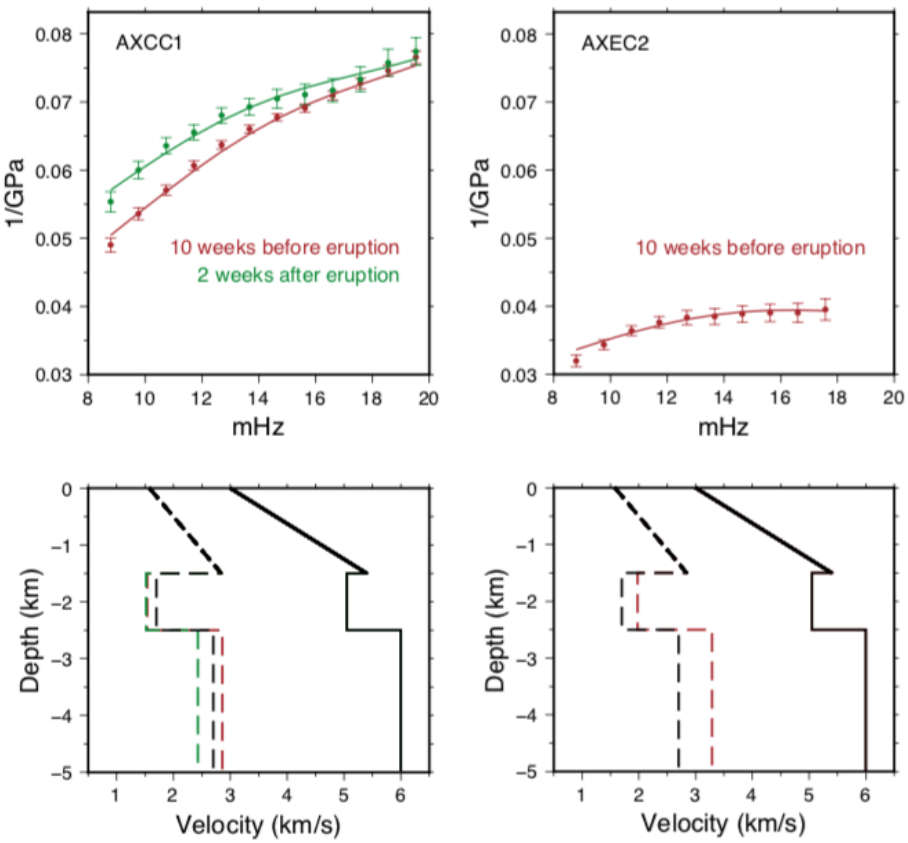

Supplemental Figure S5. Seafloor compliance data (top panels) and 1D velocity models (bottom panels) for weekly data selected before the eruption of April 25, 2015, and after. As described in Figure S4, the crust continues to 11 km depth. The data following the eruption is missing from AXEC2 could not be calculated due to low signal coherence (see text).

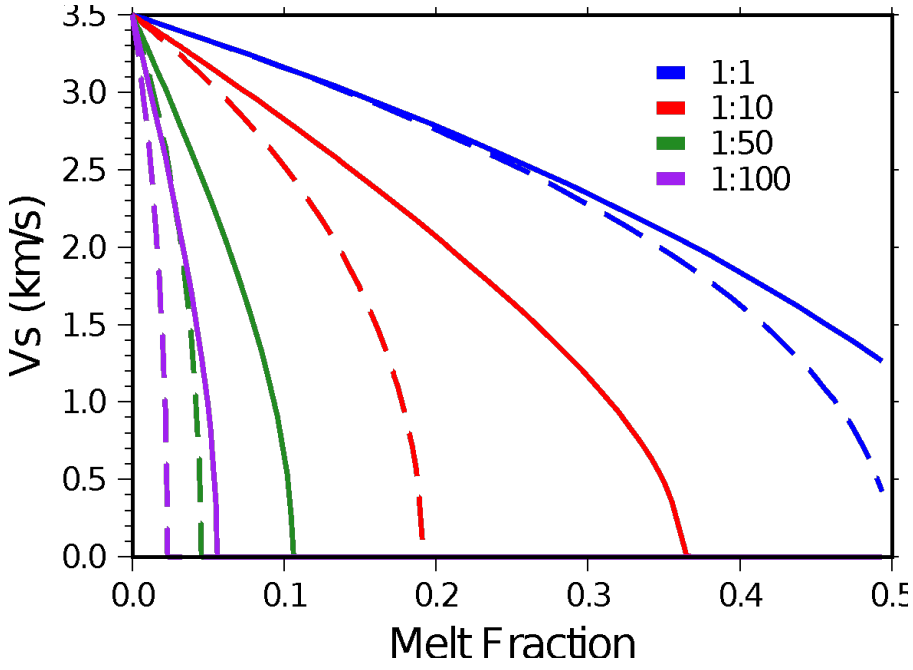

Supplemental Figure S6. Apparent Vs as a function of melt fraction and geometry computed using the formulation of Schmeling et al (2012) assuming spheroidal inclusions with aspect ratios of 1:1, 1:10, 1:50, and 1:100. The solid lines represent the effect of completely isolated melt inclusions, while the dashed lines represent completely connected melt inclusions. In our modeling we used basalt properties of Vp=6.4 km/s, Vs=3.5 km/s, and p=2.97 g/cc and basaltic melt properties of Vp=2.35 km/s, Vs=0 km/s, and p=2.7 g/cc. These values were chosen to provide melt calculations consistent with those of Arnulf et al (2018). The melt configurations detailed in the text were chosen to be consistent with our results for Vs and the Vp results of Arnulf et al (2018).